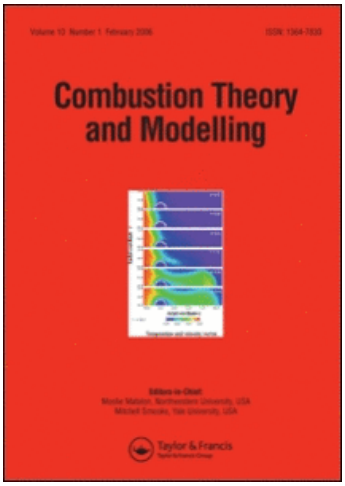

Combustion Theory and Modelling
Publication details, including instructions for authors and subscription information:
http://www.informaworld.com/smpp/title~content=t713665226

Radiation characteristics and turbulence-radiation interactions in sooting turbulent jet flames

R. S. Mehta [a]; M. F. Modest [a]; D. C. Haworth [a]
[a] Department of Mechanical and Nuclear Engineering, The Pennsylvania State University, University Park, PA, USA

Online publication date: 16 March 2010

To cite this Article Mehta, R. S., Modest, M. F. and Haworth, D. C.(2010) 'Radiation characteristics and turbulence-radiation interactions in sooting turbulent jet flames', Combustion Theory and Modelling, 14: 1, 105 — 124
To link to this Article: DOI: 10.1080/13647831003660529
URL: http://dx.doi.org/10.1080/13647831003660529

Combustion Theory and Modelling
Vol. 14, No. 1, 2010, 105–124

Taylor & Francis
Taylor & Francis Group

Radiation characteristics and turbulence–radiation interactions in sooting turbulent jet flames

R.S. Mehta,*† M.F. Modest‡ and D.C. Haworth

Department of Mechanical and Nuclear Engineering, The Pennsylvania State University, University Park, PA 16802, USA

(*Received 25 August 2009; final version received 20 January 2010*)

A comprehensive modeling strategy including detailed chemistry, soot and radiation models coupled with state-of-the-art closures for turbulence–chemistry interactions and turbulence–radiation interactions is applied to various luminous turbulent jet flames. Six turbulent jet flames are simulated with Reynolds numbers varying from 6700 to 15, 000, two fuel types (pure ethylene, 90% methane–10% ethylene blend) and different oxygen concentrations in the oxidizer stream (from 21% O_2 to 55% O_2). All simulations are carried out with a single set of physical and numerical parameters (model constants). A Lagrangian particle Monte Carlo method is used to solve a modeled joint probability density function (PDF) transport equation, which allows accurate closure for turbulence–chemistry interactions including nonlinear soot subprocesses. Radiation is calculated using a particle-based photon Monte Carlo method that is coupled with the PDF method to accurately account for both emission and absorption turbulence–radiation interactions (TRI). Line-by-line databases are used for accurate spectral radiative properties of CO_2 and H_2O; soot radiative properties also are modeled as nongray.

For the flames that have been investigated, soot emission can be almost 45% of the total emission, even when the peak soot volume fraction is of the order of a few parts-per-million (ppm) and up to 99% of soot emission can escape the domain without re-absorption. Turbulence–radiation interactions have a strong effect on the net radiative heat loss from these sooting flames. For a given temperature, species and soot distribution, TRI increases emission from the flames by 30–60%, and the net heat loss from the flame increases by 45–90% when accounting for TRI. This is higher than the corresponding increase in radiative heat loss due to TRI in nonsooting flames. Absorption TRI was found to be negligible in these laboratory-scale sooting flames with soot levels on the order of a few ppm, but may be important in larger industrial-scale flames and in higher-pressure systems.

Keywords: turbulence–radiation interactions; luminous flames; turbulent flames; photon Monte Carlo; composition PDF methods

1. Introduction

Radiation is an important mode of heat transfer at the high temperatures encountered in reacting flows [1]. Experimental and simulation results show that radiative fluxes from

*Corresponding author. Email: rsm@cfdrc.com; ranjansm@gmail.com
†Present address: CFD Research Corporation, Huntsville, AL 35805
‡Present address: University of California, Merced, CA 95343

ISSN: 1364-7830 print / 1741-3559 online

DOI: 10.1080/13647831003660529
http://www.informaworld.com

turbulent flames can be higher by more than a factor of two compared to those calculated based on local mean values (thereby ignoring turbulent fluctuations in temperature and radiative properties of the medium). This is a manifestation of turbulence–radiation interactions (TRI) [2–4]. Simulations that included TRI are found to agree better with experimental data [5–11]. The most significant effect of accurate radiation modeling is on temperature prediction; accounting for radiation can reduce the computed peak temperatures by up to 150 K or more in nonluminous flames. This temperature reduction then affects other important quantities that are highly sensitive to the temperature field, including emissions of unburned hydrocarbons, NO_x and soot.

Radiative calculations accounting for TRI in a two-dimensional furnace were carried out by Song and Viskanta [12]. There scalar fluctuations (of species concentrations and temperature) were simulated using a joint Gaussian probability density function (PDF). Absorption TRI was neglected by invoking the optically thin fluctuation approximation (OTFA) [13]. Results showed increased radiative fluxes by up to 80% with consideration of TRI when the flame occupied a large portion of the combustion chamber. Hartick *et al*. [14] extended the approach to an enclosed diffusion flame with an assumed joint PDF for the mixture fraction and chemical heat release rate. They concluded that turbulence–radiation interactions had only a small influence on the spatial distribution of temperature and other scalar fields. However, the lower temperatures significantly reduced the local NO_x production. Krebs *et al*. [15] showed that scalar fluctuations increased radiative emission at short wavelengths, and that concentration fluctuations tended to make the medium more transparent (i.e., more optically thin).

Most of the studies above treated TRI in a fairly approximate fashion: for example, using an assumed shape joint PDF for species concentration and temperature fluctuations. Instead of an assumed joint PDF, Mazumder and Modest [16, 17] solved a modeled joint velocity-composition PDF equation [18] for the simulation of a bluff-body stabilized methane–air flame. The OTFA was invoked (i.e., absorption TRI neglected) and emission TRI was determined using the transported PDF method. Similarly, Li and Modest [8, 9] used a hybrid finite-volume/composition PDF method to study TRI in methane–air jet diffusion flames. They undertook a detailed investigation of the effect of different parameters on TRI, including the Reynolds number, optical thickness, and Damköhler number. The OTFA was invoked so that only emission TRI was considered. Full-spectrum correlated k-distributions were used for accurate spectral property modeling, and the P_1-approximation was employed as the RTE solver [8,9]. Raman *et al*. [19] employed a hybrid finite volume/PDF Monte Carlo method to study partially premixed methane–air flames and obtained good agreement with experiment. Emission TRI was accurately modeled, while the OTFA was invoked to neglect absorption TRI. Wang *et al*. [20] studied nongray soot radiation in a sooting propane–air flame. A simple turbulent combustion model was used and there was no accounting for TRI. Computed soot levels were adjusted to match the experimental mean centerline soot volume fractions. They reported that nongray treatment of soot was more important than the nongray treatment of gases for their flame.

In general, the joint PDF formulation carries only one-point statistics and, hence, does not contain information about length scales or gradients [21, 22]; a separate treatment is required for absorption TRI. The first attempt to take the effects of absorption TRI into account was by Tessé *et al*. [23, 24] in their modeling of radiative transfer in a turbulent, sooty, ethylene–air jet flame. The flame was simulated using the composition PDF method of Zamuner and Dupoirieux [25]. Converged mean fields from [25] were used as a starting point for radiation calculations, and ad hoc turbulent structures then were superimposed randomly in the domain to simulate snapshots of turbulent fields. A Monte Carlo ray tracing

scheme was employed to calculate the radiative source term for each cell. With TRI the radiative heat loss was found to be about 30% of the chemical heat release. The radiative energy absorbed in the flame was comparable to the emitted energy. However, results showed a strong sensitivity to the parameters that were used to model the ad hoc turbulent structures. Very recently, Wang and Modest [11,26–28] developed and tested several Monte Carlo emission and absorption schemes for media represented by discrete particles. This circumvents the need to assume turbulent structures in the context of composition PDF methods with Lagrangian particle solution methods. This method is used in the current work and is described briefly in Section 2. The effects of TRI may be different for sooting versus nonsooting flames. In the case of nonsooting flames, TRI enhances radiative emission and radiative heat loss, and causes a decrease in the flame temperature [29]. There have been fewer studies for sooting flames and the effects of TRI are more difficult to anticipate. In the case of luminous (sooting) flames, the radiative emission from soot can be more than twice that from gases like CO_2 and H_2O, in spite of the fact that soot volume fractions in typical atmospheric-pressure laboratory-scale flames are of the order of 10^{-8}–10^{-5}; i.e., only a few ppm, at most. Therefore, accurate modeling of soot becomes a prerequisite for reasonable radiation modeling in a sooting flame [10]. Here, TRI will also depend on correlations between temperature fluctuations and soot concentration fluctuations. This investigation is one of the aims of the current work.

The objectives of this study are: (i) to quantify gas-phase radiation and soot radiation in luminous turbulent jet flames; (ii) to quantify TRI in flame emission, absorption and net heat loss in moderately sooting jet flames; and (iii) to understand the effects of neglecting turbulence–radiation interactions on prediction of various quantities. An important element of this work is that soot models that have been thoroughly validated across a wide range of laminar flames [30] are used in turbulent flames without modifications. All simulations are carried out with a single set of physical and numerical parameters (model constants).

2. Physical and numerical models

The physical models and numerical algorithms used here are the same as those used in [10]. Here only the essential aspects of the models are reviewed. Additional details of the models can be found in [10].

2.1. *Formulation*

The governing equations for mean quantities [31] include transport equations for mass, momentum, species and absolute enthalpy (energy). Additional modeled equations are needed to provide turbulence scale information. For example, a conventional two-equation k-ε turbulence model has been shown to provide reasonable accuracy for the simple jet flames that are considered here.

Composition PDF methods are a class of transported PDF methods, where physical scalars including temperature (or absolute enthalpy) and species concentrations are treated as random variables (see [32] and [18] and references therein). The joint PDF of these scalars is then a function of spatial location $\mathbf{x}$ and time t. Turbulent diffusion is modeled based on the gradient-diffusion hypothesis. The mean velocity fields and turbulent diffusivities are obtained using the standard k-ε equations. A composition PDF approach is used here, and the species and enthalpy transport equations are solved in a Lagrangian framework using Monte Carlo methods. Molecular mixing is modeled using the Euclidean-minimum-spanning-tree model [33].

Monte Carlo approaches to the solution of the PDF equation have been developed [18], which allow solutions of problems with large dimensionality (number of coupled scalars) with relative ease. The basic idea is to represent the PDF by a sufficiently large number of notional fluid particles. The mean quantities at any point in the domain are then calculated as an ensemble average over the particles in a sufficiently small neighborhood. The algorithm employed here was developed by Pope and coworkers [18,34,35] and by Subramaniam and Haworth [36]. An algorithm developed by Zhang and Haworth [37] to ensure consistency between the values obtained by a finite volume (FV) solution and Monte Carlo solution is also implemented. The composition PDF method has been extended to include soot scalars (moments) as part of the composition space, thereby capturing the effects of turbulent fluctuations on the highly nonlinear soot subprocesses [10].

A systematically reduced 33-species reaction mechanism containing 205 elementary reactions is used to model gas-phase kinetics [38]. This mechanism was found to perform satisfactorily in predicting soot volume fractions in laminar premixed and opposed-flow-diffusion ethylene–air flames across a broad range of conditions [30]. The molecular transport properties and thermochemistry have been implemented using TRANSPORT [39] and CHEMKIN-II [40], respectively; these have been interfaced with the underlying CFD code [37].

2.2. *Soot formation*

Soot formation is complex and can be divided into several subprocesses: (i) nucleation of soot particles, when they acquire characteristics different from the gas phase; (ii) surface growth/oxidation of soot particles due to reactions with the gas phase; and (iii) particle coagulation/aggregation due to collisions between soot particles. All of these processes occur simultaneously and need to be modeled accurately [41].

Soot kinetics refers to interaction of soot particles with the surrounding gas phase. A simplified nucleation mechanism based on local acetylene (C_2H_2) concentration proposed by Lindstedt and coworkers [42–44] is used here. Soot surface growth models have been an active area of research for several decades [45]. Frenklach and Wang [46,47] proposed chemical similarity, postulating that chemical reactions taking place on the soot particle surface are analogous to those for large polycyclic aromatic hydrocarbons. Soot surface oxidation is due to attack by OH radicals and oxygen [48].

Soot particle dynamics refers to interactions between soot particles, and can be treated in different ways. Here a method of moments with interpolative closure has been used [49]. Three-to-six moments have been found to be sufficient in previous modeling studies of laminar premixed flames [30,47,50] and opposed-flow diffusion flames [30,51]. Since the current study is limited to atmospheric-pressure flames, it is expected that soot particles will remain primarily spheroidal; hence aggregation is not considered. The model has shown uniformly good agreement between the computed and measured soot levels for turbulent jet flames [10].

2.3. *Radiation*

Radiation is governed by the complex integro-differential radiative transfer equation (RTE) in five dimensions [1]. In addition, the spectral behavior of the absorption coefficient of the medium depends on its composition and local concentrations of selectively absorbing/emitting combustion gases such as water vapor, carbon dioxide and particulate matter such as soot [20,52]. The radiative source term in the absolute enthalpy equation represents

the local net volumetric gain of thermal energy due to both emission and absorption, and can be expressed as [1]

$$S_{\text{rad}} = -\nabla \cdot \underline{q}^R = \int_0^\infty \kappa_\eta \left(\int_{4\pi} I_\eta d\Omega - 4\pi I_{b\eta} \right) d\eta, \tag{1}$$

where $\underline{q}^R$ is the radiative heat flux, $\kappa_\eta = \kappa_\eta(\underline{Y}, T, p)$, is the spectral absorption coefficient of the radiating medium (mixture), which may be a function of temperature T and species concentrations (expressed as mass fractions $\underline{Y}$) of the radiating medium. Here I_η is the spectral radiative intensity, and $I_{b\eta}$ is the Planck function or spectral blackbody intensity. The subscript η denotes spectral dependence and Ω is the solid angle. To determine I_η it is necessary to solve the RTE and this can be done using various methods, including: (i) spherical harmonics methods [8, 16]; (ii) discrete-ordinates methods [53]; or (iii) photon Monte Carlo (PMC) methods [11, 54, 55]. A powerful feature of the PMC methods is their ability to handle complex problems with relative ease.

2.3.1. *Turbulence–radiation interactions*

The absorption coefficient κ_η depends nonlinearly on both species concentrations and temperature. Therefore, the mean of the product of κ_η and $I_{b\eta}$ is not equal to the product of their means: $I_{b\eta}$

$$\langle \kappa_\eta I_{b\eta} \rangle = \langle \kappa_\eta \rangle \langle I_{b\eta} \rangle + \langle \kappa'_\eta I'_{b\eta} \rangle \neq \kappa_\eta(\tilde{\underline{Y}}, \tilde{T}, p) \langle I_{b\eta} \rangle, \tag{2}$$

$$\langle I_{b\eta} \rangle \neq I_{b\eta}(\tilde{T}), \tag{3}$$

and similarly,

$$\langle \kappa_\eta I_\eta \rangle = \langle \kappa_\eta \rangle \langle I_\eta \rangle + \langle \kappa'_\eta I'_\eta \rangle \neq \kappa_\eta(\tilde{\underline{Y}}, \tilde{h}) \langle I_\eta \rangle. \tag{4}$$

Here $\tilde{Q} = \langle \rho Q \rangle / \langle \rho \rangle$ denotes a Favre-averaged quantity and $\langle Q \rangle$ denotes a Reynolds-averaged quantity.

The essence of TRI modeling is to accurately estimate the left-hand sides of Equations (2) and (4). In these equations, $< \kappa'_\eta I'_\eta >$ represents the correlation between the fluctuating absorption coefficient and spectral incident intensity, and $< \kappa'_\eta I'_{b\eta} >$ represents the correlation between the fluctuating absorption coefficient and the local blackbody intensity. Following Li [56], these two correlations are loosely defined as absorption coefficient–incident intensity correlation (absorption TRI) and absorption coefficient–black body intensity (Planck function) correlation–emission TRI, respectively.

2.3.2. *Radiative properties and RTE solver*

For combustion applications where joint PDF methods [18] are used, the medium often is represented by notional particles, and traditional Monte Carlo ray-tracing schemes developed for continuous media are no longer useful for such stochastic media. Recently, Wang and Modest [26] developed several emission and absorption schemes for media represented

by discrete particles. The method was extended to achieve line-by-line accuracy in radiative property calculations with little increase in computational cost [27]. The PMC simulates the process of emitting radiation by releasing representative photon bundles (rays) in random directions, which are traced until they are absorbed (completely) at certain points in the medium or escape from the domain. An energy-partitioning scheme is utilized which reduces statistical error, compared to standard Monte Carlo [1]. In media represented by discrete particles, the ray energy is distributed over all the particles with which the ray interacts when the energy-partitioning method is employed [26]. The particle-based PMC method can be employed to evaluate both the local emission ($\langle 4\pi\kappa_\eta I_{b\eta}\rangle$) and the absorption of incident radiation ($\langle \kappa_\eta I_\eta \rangle$) exactly without further assumptions [11].

The effects of TRI may be different for sooting and nonsooting flames. In the case of nonsooting flames, it has been shown that TRI enhances radiative emission and radiative loss, and causes a decrease in the flame temperature. In sooting flames, TRI will also depend on correlations between temperature fluctuations and soot concentration fluctuations, which may either be positive or negative, depending on the values of temperature, soot concentration, wavelength and turbulence intensity.

Soot particles are assumed to be spherical and small compared to the wavelengths of interest. Rayleigh theory is used to obtain expressions for both the absorption and scattering coefficients of the soot particles [1]. The complex index of refraction of soot is modeled using correlations developed by Chang and Charalampopoulos [57]. At high pressures the soot particles are expected to be larger and have a mass-fractal like geometry [58]. In such a scenario, more sophisticated soot radiative property models will be required [59].

2.4. *Experimental data*

Seven atmospheric-pressure luminous, nonpremixed turbulent jet flames have been simulated (Table 1). Flame I is a turbulent jet flame studied experimentally by Coppalle and Joyeux [60] with a jet Reynolds number of 11, 800. Temperature and soot volume fractions were measured simultaneously using two-color pyrometry and extinction measurements, respectively. Flame II was studied experimentally by Kent and Honnery [61]. Extinction measurements were carried out along secants and radial soot volume fractions were "estimated" using an Abel inversion technique [62]. Temperatures were measured directly using uncoated thermocouples, and a radiation correction was applied using a surface emissivity of 0.2. Turns and coworkers [20, 52, 63–65] undertook detailed characterization of turbulent jet flames with oxygen enrichment (Flames III–VI). They conducted a number of experiments to understand how key parameters affect the soot, radiation and emission characteristics of jet flames over a range of oxygen indices from 21% (air) to 100% (pure O_2). Line-of-sight laser extinction measurements were used to measure an equivalent soot volume fraction at different axial locations. Radiation measurements were made using a wide-angle (150°) window. Radiative heat flux measurements were made at 100 mm intervals along the wall, and then integrated to determine the total radiative heat loss. Duct walls were coated with high-temperature infrared-black paint. Radiant heat loss as a fraction of the total chemical heat release rate was also reported [63, 64]. These flames have been simulated using a comprehensive, state-of-the art models by Mehta *et al*. [10]. In the current study, all the submodels except those for TRI are unaltered compared to [10] and the effects of TRI are isolated and quantified. Flame VII is a scaled-up version of Flame II (see Section 3.5).

Table 1. Radiation characteristics of Flames I–VI (frozen-field analysis). The percentage numbers are evaluated with respect to values provided in Table 2.

Flame	Fuel	Oxidizer	Jet dia. (mm)	Reynolds number	Ref.	Emission TRI (%)	Increase in heat loss due to TRI (%)	Absorption TRI (%)	Soot emission (%)	Gas emission (%)	Gas emission re-absorbed (%)	Soot emission re-absorbed (%)
I	Ethylene	Air	4	11,800	[60]	39	69	0.44	39	61	54	8
II	Ethylene	Air	3	15,100	[61]	57	88	0.07	43	57	45	7
III	Blend	Air	3	6700	[64]	41	62	0.32	5	95	46	3
IV	Blend	30% O_2	3	6700	[64]	32	50	0.96	9	91	42	3
V	Blend	40% O_2	3	6700	[64]	44	54	0.17	7	93	41	3
VI	Blend	55% O_2	3	6700	[64]	38	44	0.57	4	96	35	1

Blend: 90% methane–10% ethylene.

Table 2. Computed volume-integrated quantities of Flames I–VI (frozen-field analysis).

Flame	Emission with TRI (kW)	Emission without TRI (kW)	Heat loss with TRI (kW)	Heat loss without TRI (kW)	Gas emission (kW)	Soot emission (kW)	Loss due to gas emission (est.) (kW)	Loss due to soot emission (est.) (kW)
I	6.17	4.42	3.97	2.34	3.73	2.44	1.72	2.24
II	7.63	4.88	5.46	2.89	4.35	3.28	2.37	3.04
III	2.24	1.59	1.27	0.77	2.14	0.1	1.15	0.1
IV	3.41	2.58	2.1	1.39	3.11	0.3	1.82	0.29
V	3.32	2.31	2.05	1.33	3.1	0.22	1.82	0.21
VI	3.02	2.18	2.01	1.38	2.9	0.12	1.88	0.12

2.5. *Numerical model*

A three-dimensional wedge-like grid system is employed to simulate the axisymmetric flame by applying periodic boundary conditions on the lateral surfaces, with a wedge angle of 10°; the dimensions in x- (radial) and z- (axial) directions are $30d_j$ and $250d_j$, where d_j is the fuel jet diameter respectively. The grid is fine near the fuel jet to accurately resolve large local gradients in the mixing region, and is coarser in the coflow air region and downstream to save computational time. With composition PDF methods, it has been found that approximately 30 particles per cell are sufficient to resolve the turbulent fluctuations in the flame. Equilibrium chemistry is used in a small region close to the fuel jet exit, to stabilize the flame. For statistically steady flows, the simulations are run in a transient manner until the mean quantities become independent of time. Time averaged quantities are estimated as,

$$\langle Q_{c,n} \rangle = x \langle Q_{c,n,p} \rangle + (1 - x) \langle Q_{c,n-1} \rangle, \tag{5}$$

where $\langle Q_{c,n,p} \rangle$ is the ensemble average in cell c at time-step n, $\langle Q_{c,n} \rangle$ is the time-averaged quantity in cell c at time-step n and $0 \leq x \leq 1$ is a blending factor. This method was found to give smooth mean scalar fields which evolve towards the correct value as the simulation times are increased. The advantage of such a scheme is that no memory is required to store time histories, while a disadvantage is that different time-steps are not weighted equally. Approximately 100, 000 photon bundles at every time-step was found to be sufficient for statistically stationary configurations. The tempering scheme used in Equation (5) allows using a small number of photon bundles at every time-step. Additional details about the approach can be found in [10].

3. Results and discussion

3.1. *Radiant fractions*

Radiant heat loss from Flames I–VI as fraction of the total chemical heat release (radiant fraction) are shown in Figure 1. The chemical heat release is calculated based on the lower heating values (i.e., gaseous water-vapor in the products) for methane and ethylene estimated to be 50.0 MJ/kg and 47.1 MJ/kg, respectively. The experimental radiant heat fractions for Flames III–VI increase with increasing oxygen content due to increasing flame temperature. Computed radiant fractions decrease for Flames V and VI due to smaller computed flame

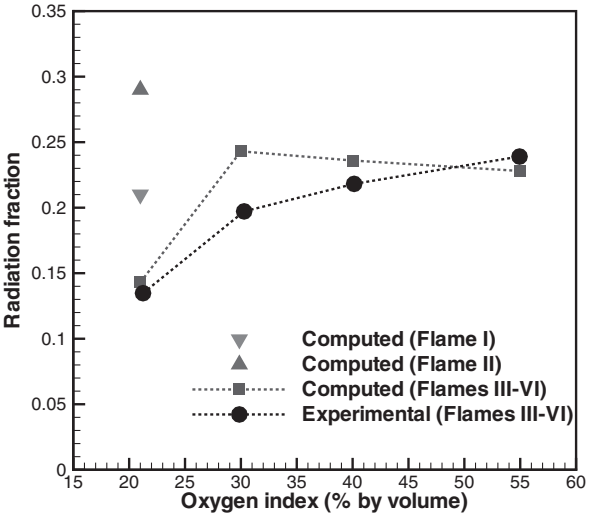

Figure 1. Computed and measured (when available) radiant fractions for Flames I–VI.

lengths [10]. In general, computed radiant fractions are reasonable and agree well with experimental data where available.

3.2. *Separating TRI*

In general, it is not possible to separate the effects of turbulence–radiation interactions when conducting physical experiments. An important advantage of the physics-based simulation techniques used here is the ability to quantify effects of various subprocesses on the overall flame structure and phenomena of interest. In the stochastic solution of transported PDF equations, an ensemble of particles through the entire domain then is viewed as a snapshot of the turbulent flow-field [11]. An appropriate approach to isolate the effects of TRI then is to solve the RTE based on the mean fields (neglecting TRI) and also based on the particle fields in a statistically steady state (including TRI). The difference between these two solutions gives contributions by TRI.

To systematically isolate TRI effects, a frozen field study is carried out. Ten uncorrelated PDF-particle fields are extracted from the fully coupled, full-TRI simulation after achieving statistical convergence (or statistically steady state). The PMC method is used in conjunction with the frozen fields by considering full TRI (emission and absorption both based on particle values), partial TRI (only emission is based on particle values) and no TRI (emission and absorption are both based on cell mean quantities), to estimate the corresponding radiative transfer from the flames. It is emphasized that in all cases the turbulence–chemistry interactions are fully accounted for (chemical and soot source terms are computed using particle values). An appropriate metric to gauge the net effect of various TRI modes on the radiative transfer from a flame is to estimate the total emission from the flames evaluated with and without TRI effects,

$$\dot{Q}_{\text{emi}} = \int_V q_{\text{emi}} dV \tag{6}$$

and the net heat loss from the flame evaluated with and without TRI effects,

$$\dot{Q}_{\text{net}} = \int_V \nabla \cdot \underline{q_R} dV \tag{7}$$

where q_{emi} is the local volumetric radiative emission and $\nabla \cdot \vec{q_R}$ is the local radiative heat loss per unit volume.

Another important aspect is quantification of absorption TRI, or the correlation between the absorption coefficient and incident intensity. Absorption TRI can be separated based on the following equation:

$$\underbrace{\langle 4\pi\kappa I_b\rangle - \langle \kappa G\rangle}_{\text{Full TRI}} = \underbrace{\langle 4\pi\kappa I_b\rangle - \langle\kappa\rangle\langle G\rangle}_{\text{Partial TRI}} - \langle k'G'\rangle \tag{8}$$

which results in

$$\underbrace{\langle k'G'\rangle}_{\text{Absorption TRI}} = \underbrace{\langle 4\pi\kappa I_b\rangle - \langle\kappa\rangle\langle G\rangle}_{\text{Partial TRI}} - \underbrace{\langle 4\pi\kappa I_b\rangle + \langle\kappa G\rangle}_{\text{Full TRI}} \tag{9}$$

where $G = \int_{4\pi} I d\Omega$ is the net incident radiation integrated over all directions at a given point, and we have integrated over all wavenumbers. The difference in the computed heat loss based on full TRI and partial TRI can be attributed solely to absorption TRI (Equation 9).

The results of different TRI treatments on volume-integrated quantities characterizing Flames I–VI are summarized in Table 1 and the corresponding absolute values in Watts are shown in Table 2. Net emission increases by $\sim$ 30–60% when accounting for TRI. When considering full TRI, the predicted heat loss is $\sim$ 40–90% higher than that obtained without including TRI. The percentage values are based on values obtained when considering full TRI treatment. Absorption TRI values are shown in Table 1 as a percentage of absorption with TRI. Absorption TRI is always negligible for the laboratory-scale flames studied in the current work. Thus, it should be possible to neglect absorption TRI for relatively small flames, irrespective of whether they are sooting flames or not. This finding has important implications on modeling studies conducted previously and those that use RTE solvers which cannot account for absorption TRI accurately.

3.3. *Gas and soot radiation*

Analysis of flame radiation without the effects of radiation feeding back to modify the flowfield can also be used to obtain first-order estimates of the importance of soot radiation compared to gas-phase radiation. These values are also reported in Table 1. Soot emission is as high as 46% of the total emission (soot and gas combined) for Flame II and is less than 5% of the total emission for Flames III and VI. Molecular gases emit and absorb across specific spectral bands [1]. On the other hand, soot radiation is significant almost over the entire infrared spectrum, absorbing and emitting with a continuous absorption coefficient. If it is further assumed that a relatively very small portion of gas emission is absorbed by soot, and that very little of the continuous spectrum soot emission is absorbed by the gases, then the contribution of soot radiation to the net heat loss from the flame can be estimated.

Table 1 also shows the fraction of gas and soot emission that is re-absorbed in the computational domain. Approximately 40–50% of the radiation emission from the participating

Table 3. Comparison of key computed metrics for Flame II, with and without TRI (fully coupled analysis).

Description	TRI	No TRI
Emission weighted average temperature (K)	1644	1888
Net radiative loss (W)	5450	2473
Peak centerline mean soot volume fraction (ppm)	1.05	0.88
Peak centerline mean temperature (K)	1863	1938

gases is re-absorbed in the domain. This is due to the fact that combustion gases emit and absorb in specific spectral bands. However, more than 90% of soot emission leaves the domain because continuum radiation from soot "sees" a relatively transparent medium. A possible implication of these results (Table 1) is that even a gray soot radiative property model may suffice for predictions within experimental uncertainties. A gray soot model can reduce the effort of incorporating soot radiation into an existing RTE solver, or a PMC method. Gas radiation however, has to be treated in a nongray fashion to obtain sufficient accuracy. However, frozen-field analysis was not carried to separate out different radiation effects.

3.4. *Simulations without TRI*

So far, the effects of TRI have been isolated by comparing radiation quantities computed using particle values in simulations that include TRI. In contrast, a fully coupled solution without TRI results in a different flame structure, which feeds back into the flow solver through the mean density field. Here radiative properties are evaluated based on cell mean values of concentrations and temperature. All other model parameters are kept the same as those used in simulations with full TRI; in particular, turbulence–chemistry interactions are still fully accounted for by computing chemical source terms based on particle values. Computed and measured centerline mean temperature profiles for Flame II are shown in Figure 2. Neglecting TRI increases the peak temperature by 70 K, and the computed peak centerline mean soot volume fraction is reduced from 1.2 ppm to just over 0.8 ppm. Other

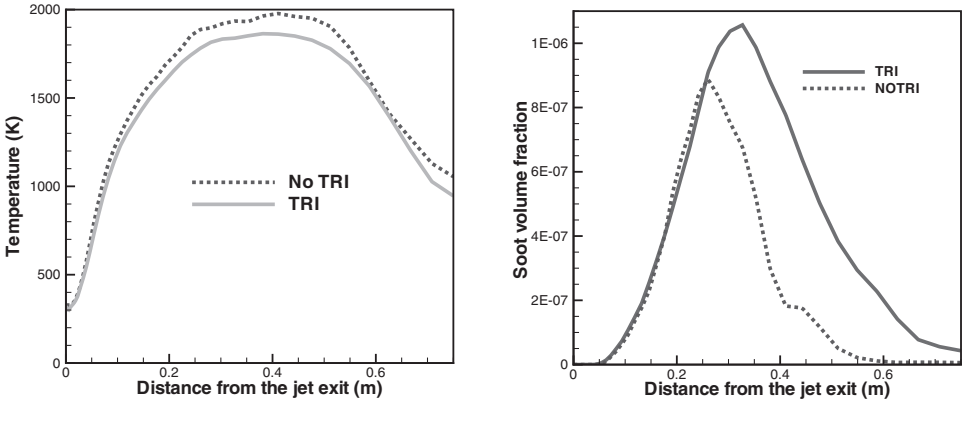

Figure 2. Comparison between model predictions for the centerline mean temperature and soot volume fractions for Flame II, with and without TRI.

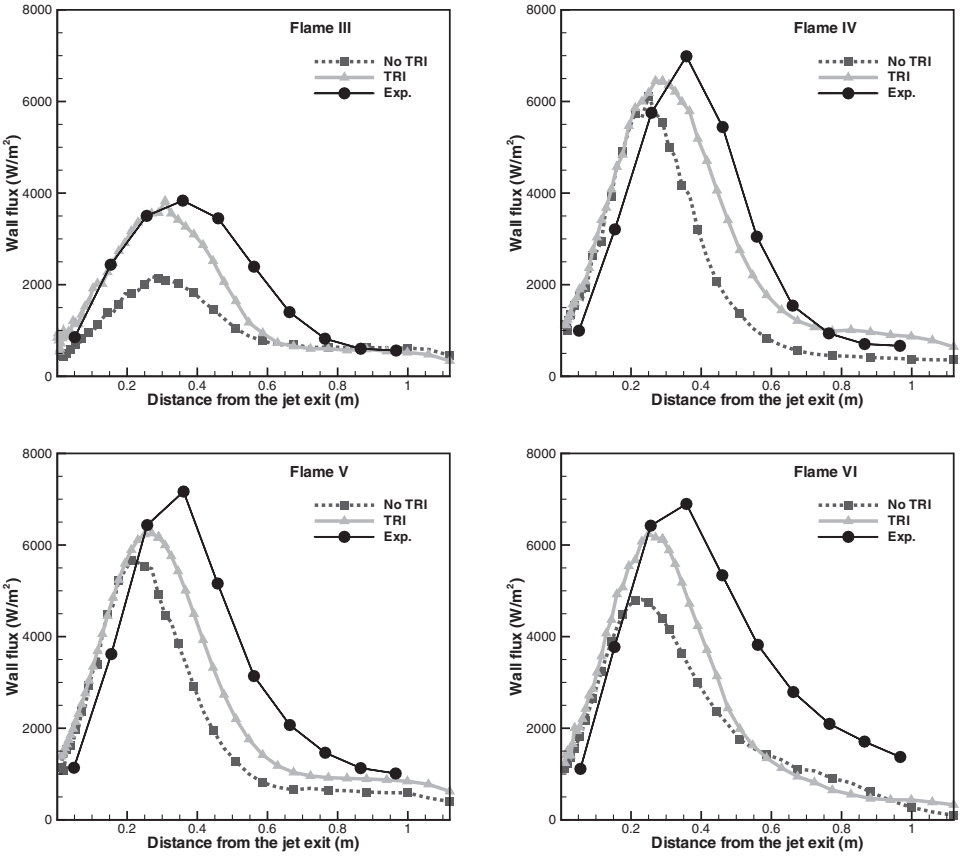

Figure 3. Predicted and measured wall fluxes for Flames III–VI.

key metrics for Flame II, with versus without TRI, are compared in Table 3. The flame is hotter when TRI is not included while the net radiative loss is still lower.

The net effect of increased temperatures also appears in the soot predictions which are the net result of two effects: (i) soot surface growth is inversely proportional to temperature, and (ii) increased temperature also increases oxidation rates for the soot. At the same time, increased temperatures also increase the kinetic rates of all reactions, including soot growth reactions and, hence, the net effect of increased temperatures on the flame structure and soot yield is generally difficult to predict.

Predicted wall heat fluxes for Flames III–VI, with versus without TRI, are shown in Figure 3. Neglecting TRI consistently under-predicts the radiative wall heat flux and, consequently the radiative losses from the flame. Peak mean centerline temperatures are $\sim$ 20–60 K higher for these flames when TRI are excluded. Increased temperatures have a marked effect on the kinetic rates of the gas-phase reactions as well as on soot formation rates. Predicted equivalent soot volume fractions for Flames III–VI are shown in Figure 4. Computed soot volume fractions decrease by as much as a factor of three, and are in better agreement with experiment, when TRI are considered. Some key metrics for the oxygen enriched Flames III–VI are shown in Table 4. The emission-weighted average temperature

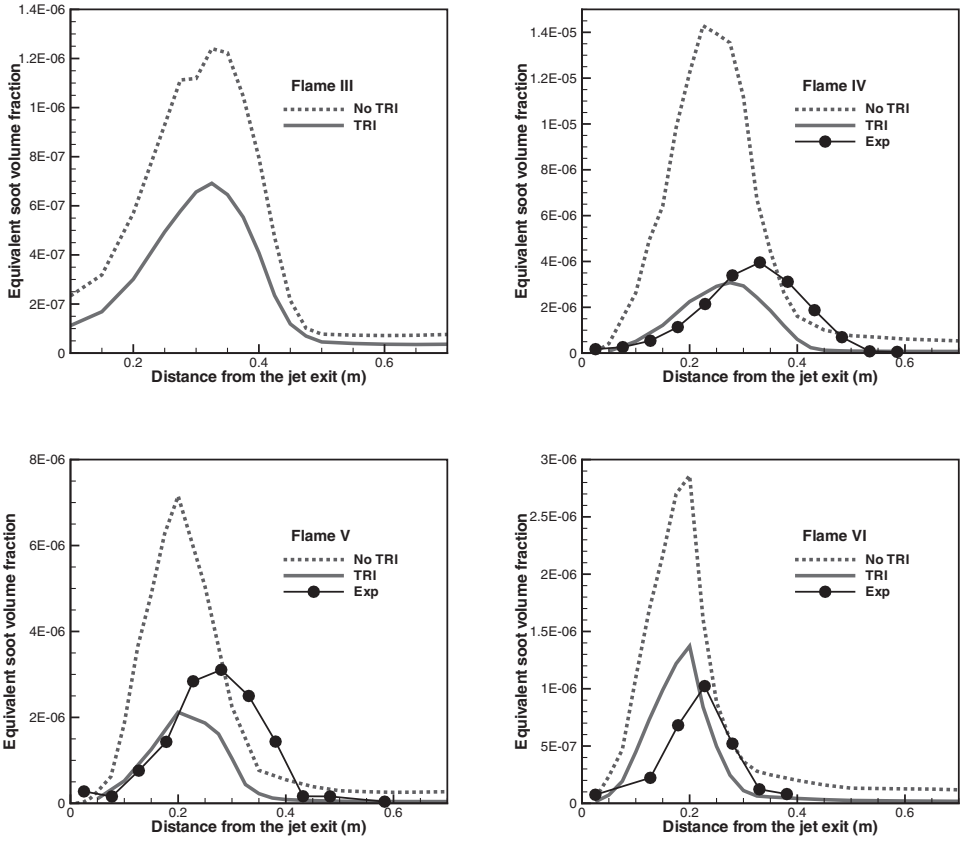

Figure 4. Predicted and measured equivalent soot volume fractions for Flames III–VI.

is defined as [66]

$$T_{\text{emi,av}} = \frac{\int_V \kappa_p \sigma T^5}{\int_V \kappa_p \sigma T^4}, \tag{10}$$

where κ_p is the total Planck-mean absorption coefficient and T is the temperature. Table 4 shows that $T_{\text{emi,av}}$ is consistently higher when neglecting TRI, and the net radiative loss from these flames is $\sim$ 30–50% lower when neglecting TRI. The emission-weighted average domain temperature can be interpreted as a metric showing the overall radiative emission tendency of various flames.

3.5. *Modeling a large flame (VII)*

Negligible absorption TRI was found for all the laboratory-scale flames studied here. It is expected that absorption TRI may be significant in sufficiently optically thick flames. Since Flame II yielded the highest soot volume fractions of the flames considered here, a scaled-up Flame II is simulated with jet diameter $d_j = 96$ mm (a factor of 32 larger than Flame II). The jet velocity is maintained at 52.5 m/s, while the dimensions of the mesh are increased by a factor of 32 in each direction.

Table 4. Comparison of key metrics for oxygen enriched Flames III–VI with and without TRI (fully coupled analysis).

	Flame III		Flame IV		Flame V		Flame VI	
Description	TRI	No TRI	TRI	No TRI	TRI	No TRI	TRI	No TRI
Emission weighted average temperature (K)	1296	1381	1586	1682	1709	1783	1922	1978
Net radiative loss (W)	1250	853	2101	1550	2051	1598	2000	1795
Peak equivalent soot volume fraction (ppm)	0.68	1.23	3.6	14.2	2.11	7.09	1.36	2.84
Peak centerline mean temperature (K)	1790	1840	2112	2150	2418	2451	2632	2665

Caution should be exercised in interpreting the results. The following assumptions have been made, and can affect the computed results to a great extent.

(1) Buoyancy effects are neglected, even though the flame is large enough for buoyancy effects to be significant, as seen in most industrial-scale burners and large fires.
(2) In practical large-scale burners, a ring of small-diameter jets is used in place of one large-diameter jet to facilitate better mixing of the fuel and oxidizer streams. This may result in different flame structure than computed here.
(3) Large flames exhibit vortex shedding and other large unsteady structures, which cannot be captured using the Reynolds-averaged flow model used here.

Nevertheless, it is expected that radiation and TRI results will provide useful insight.

Computed mean centerline temperatures and soot volume fractions with different radiation treatments are shown in Figure 5. Neglecting TRI over-predicts the temperature along the entire axis, and the peak mean temperature is approximately 40 K higher than with full TRI. Results with partial TRI (i.e., only emission TRI) show higher temperatures in some regions than even the full TRI case. Neglecting absorption TRI underpredicted the absorption. This was an unexpected result, and further investigation is described in Section 3.6. The global radiant fraction for Flame VII was calculated to be 32% of the chemical heat release, which is similar to that of Flame II.

3.6. *Frozen field analysis: Flame VII*

A frozen field analysis for the large Flame VII was performed for further insight into TRI. Global results and predictions of both emission and absorption TRI are shown in Table 5. Emission TRI contributes approximately 20% to the total emission, and this is lower than expected (with values closer to 30% in Flames I–VI). At the same time, there is significant absorption TRI and it is negative (i.e., the medium becomes more transmissive due to turbulent fluctuations).

To understand the negative absorption TRI and the importance of gas and soot radiation in the overall radiative losses from the flame, the frozen field analysis is utilized to separate gas radiation effects from overall radiation. Table 5 also shows gas and soot contributions

Table 5. Radiation quantities for Flame VII (frozen-field analysis).

	Emission with TRI (MW)	Emission without TRI (MW)	Heat loss (full TRI) (MW)	Heat loss (partial TRI) (MW)	Heat loss (no TRI) (MW)	Emission TRI %	Absorption TRI (%)	% of total emission (Full TRI)	% of radiation re-absorbed (Full TRI)
Total Radiation	27.79	22.12	6.13	4.87	1.89	20.42	−5.83	100	78
Gas-phase radiation	8.83	5.43	1.2	1.4	0.64	38.48	2.6	32	86
Soot radiation	18.96	16.69	4.93	3.47	1.25	12.02	−10.41	68	74

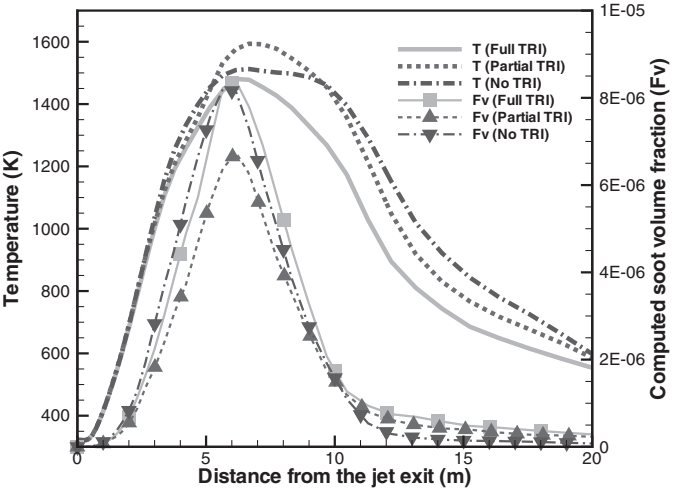

Figure 5. Computed mean centerline profiles of temperature and soot volume fraction with different radiation treatments for Flame VII.

to total radiation. Soot emission is more than twice that of the gas-phase emission. This is despite the fact that the sooting region is much smaller than that of the participating gases. Almost 85% of all the gas-phase emission is reabsorbed in the computational domain. This is significantly higher than the gas-phase re-absorption in laboratory-scale flames, because the optical thickness of the entire system is much higher than previously encountered. Similarly, almost 75% of the soot emission is re-absorbed in the computational domain, compared to a maximum of approximately 10% in laboratory-scale flames. In addition to the larger dimensions, the higher mean soot volume fractions of 10 ppm also result in a optically very thick core region near the centerline. At these optical thicknesses, the often-used approximations of gray gas, gray soot and negligible reabsorption clearly break down and, hence, cannot be used.

Table 5 shows the results of separating TRI effects for the gas-phase and soot. Emission TRI increases total emission from the flame gases by almost 40% compared to the case without TRI, which is comparable to values that have been reported in the literature (see [29] and references therein). Absorption TRI accounts for approximately 2% of the total absorption. Thus, absorption TRI in gas-phase radiation can be reasonably neglected. This shows that absorption TRI are generally not important when dealing with gas-phase radiation in reacting flows, even for large flames.

Emission and absorption TRI for soot are also shown in Table 5. Emission TRI is approximately 12% compared to around 35% seen in Flames I–VI and gas-phase emission TRI in Flame VII studied so far. Negative absorption TRI of approximately 10% is reported for the soot. This finding is opposite to the trend seen in gas-phase radiation. In the optically thick limit, $\int_\Omega I\,d\Omega$ goes to $G \Rightarrow 4\pi I_b$, implying that $\kappa G \rightarrow 4\pi\kappa I_b$, and $\kappa' G' \Rightarrow 4\pi\kappa' I_b'$. Thus, in optically extremely thick situations, absorption TRI must balance emission TRI. However, in the optically intermediate domain, when the turbulent eddies are neither sufficiently optically thin to neglect absorption TRI, nor sufficiently thick to approach the limiting solution, it is difficult to predict the behavior of absorption TRI. Another strong possibility is that there are regions in the flame where the soot absorption coefficient (due to soot volume fractions) reduces with an increase in temperature. This can happen in relatively

oxygen-rich regions, where increased temperatures increase oxidation rates and reduce the soot volume fraction. Such a negative correlation is still not enough to make emission TRI (for soot only) negative, as the temperature self-correlation more than compensates for the negative correlation. In the end, the net effect is a positive emission TRI, though much smaller than the values seen in gas-phase-only radiation. However, for absorption TRI, such a compensating mechanism is not available and hence it follows the negative trend in a stronger fashion. A fruitful direction of research would be to investigate whether modifying the soot model to make it less sensitive to temperature fluctuations changes the computed absorption TRI.

4. Conclusion

In general, turbulence–radiation interactions have strong effects on the net radiative heat loss from sooting flames. For a given temperature, species and soot distribution, TRI increases emission from the flames by 30–60%. Absorption also increases, but primarily due to the increase in emission. The net heat loss from the flame increases by 45–90% when accounting for TRI. This is much higher than the corresponding increase due to TRI in nonsooting flames.

Absorption TRI was found to be negligible in laboratory-scale sooting flames with soot levels on the order of a few ppm. Modeling absorption TRI is very difficult and requires expensive RTE solvers like the particle-based PMC. Thus, if one could neglect absorption TRI even in sooting flames to a reasonable degree, other types of RTE solvers like the P_1 and discrete ordinates (DOM) could be employed as long as emission TRI is properly considered.

Soot emission was found to contribute as much as 70% of the total emission from the flames, even though soot is present only over a small part of the computational domain. Therefore, accurate soot prediction is critical for correct evaluation of radiative losses from sooting flames. For small, laboratory-scale flames, only 40–60% of gas emission leaves the domain. On the other hand, in case of soot radiation, more than 90% of the soot emission left the domain. When simulating a large flame, absorption TRI in the gas-phase radiation could be reasonably neglected. Relatively larger absorption TRI (approximately 10%) was computed for soot radiation. Simulations of sooting flames carried out without including TRI yield additional insight into the importance of TRI. Simulations that include TRI generally showed better agreement with experiments than simulations that neglected TRI.

Acknowledgment

This work has been supported, in part, by the National Science Foundation under grant #CTS-0121573 and NASA under grant #NNX07AB40A. RSM would like to thank Professor Stephen Turns of The Pennsylvania State University for fruitful discussions.

References

[1] M.F. Modest, *Radiative Heat Transfer*, 2nd edn, Academic Press, New York, 2003.
[2] G.M. Faeth, J.P. Gore, S.G. Chuech and S.M. Jeng, Radiation from turbulent diffusion flames, in C.L. Tien and T.C. Chawla, eds. *Annual Review of Numerical Fluid Mechanics and Heat Transfer*, Vol. 2, Hemisphere, Washington, DC, 1989, pp. 1–38.
[3] M.E. Kounalakis, J.P. Gore and G.M. Faeth, *Mean and fluctuating radiation properties of nonpremixed turbulent carbon monoxide/air flames*, J. Heat Transfer 111 (1989), pp. 1021–1030.

[4] J.P. Gore and G.M. Faeth, *Structure and spectral radiation properties of turbulent ethylene/air diffusion flames*, Proc. Combust. Inst. 21 (1986), pp. 1521–1531.
[5] T.H. Song and R. Viskanta, *Interaction of radiation with turbulence: Application to a combustion system*, J. Thermophys. Heat Transfer 1 (1987), pp. 56–62.
[6] R.J. Hall and A. Vranos, *Efficient calculations of gas radiation from turbulent flames*, Int. J. Heat Mass Transfer 37(17) (1994), pp. 2745–2750.
[7] S. Mazumder and M.F. Modest, *A PDF approach to modeling turbulence–radiation interactions in nonluminous flames*, Int. J. Heat Mass Transfer 42 (1999), 971–991.
[8] G. Li and M.F. Modest, *Application of composition PDF methods in the investigation of turbulence–radiation interactions*, J. Quant. Spectrosc. Radiat. Transfer 73(2–5) (2002), pp. 461–472.
[9] G. Li and M.F. Modest, *Importance of turbulence–radiation interactions in turbulent diffusion jet flames*, J. Heat Transfer 125 (2003), pp. 831–838.
[10] R.S. Mehta, D.C. Haworth and M.F. Modest, *Composition PDF/photon Monte Carlo modeling of moderately sooting turbulent jet flames*, Combust. Flame, Article in Press, doi:10.1016/j.combustflame.2009.11.009 (2009).
[11] A. Wang and M.F. Modest, *Monte Carlo simulation of radiative heat transfer and turbulence interactions in methane/air jet flames*, J. Quant. Spectrosc. Radiat. Transfer 109 (2007), pp. 269–279.
[12] T.H. Song and R. Viskanta, *Interaction of radiation with turbulence: Application to a combustion system*, J. Thermophys. Heat Transfer 1(1) (1987), pp. 56–62.
[13] V.P. Kabashnikov and G.I. Myasnikova, *Thermal radiation in turbulent flows – Temperature and concentration fluctuations*, Heat Transfer – Soviet Research 17(6) (1985), pp. 116–125.
[14] J.W. Hartick, M. Tacke, G. Fruchtel, E.P. Hassel and J. Janicka, *Interaction of turbulence and radiation in confined diffusion flames*, Proc. Combust. Inst. 26(1) (1996), pp. 75–82.
[15] W. Krebs, R. Koch, L. Eigenmann and S. Wittig, *Effect of temperature and concentration fluctuations on radiative heat transfer in turbulent flames*, Proc. Combust. Inst. 26 (1996), pp. 2763–2770.
[16] S. Mazumder and M.F. Modest, *A PDF approach to modeling turbulence–radiation interactions in nonluminous flames*, Int. J. Heat Mass Transfer 42 (1999), pp. 971–991.
[17] S. Mazumder and M.F. Modest, *Turbulence–radiation interactions in nonreactive flow of combustion gases*, J. Heat Transfer 121 (1999), pp. 726–729.
[18] S.B. Pope, *PDF methods for turbulent reactive flows*, Prog. Energy Combust. Sci. 11(2) (1985), pp. 119–192.
[19] V. Raman, R.O. Fox and A.D. Harvey, *Hybrid finite-volume/transported PDF simulations of a partially premixed methane–air flame*, Combust. Flame 136 (2004), pp. 327–350.
[20] L. Wang, M.F. Modest, D.C. Haworth and S.R. Turns, *Modeling nongray soot and gas-phase radiation in luminous turbulent nonpremixed jet flames*, Combust. Theory Model. 9(3) (2005), pp. 479–498.
[21] R.S. Mehta and M.F. Modest, *Modeling absorption TRI in optically thick eddies*, in *Proceedings of Eurotherm Seminar 78*, Elsevier, Poitiers, France, April 2006.
[22] R.S. Mehta, *Modeling of absorption coefficient–intensity correlations for optically thick eddies in turbulent reacting flows using hybrid finite volume/PDF Monte Carlo methods*, Master's thesis, The Pennsylvania State University, Department of Mechanical Engineering, University Park, PA, 2005.
[23] L. Tessé, F. Dupoirieux, B. Zamuner and J. Taine, *Radiative transfer in real gases using reciprocal and forward Monte Carlo methods and a correlated-k approach*, Int. J. Heat Mass Transfer 45 (2002), pp. 2797–2814.
[24] L. Tessé, F. Dupoirieux and J. Taine, *Monte Carlo modeling of radiative transfer in a turbulent sooty flame*, Int. J. Heat Mass Transfer 47 (2004), pp. 555–572.
[25] B. Zamuner and F. Dupoirieux, *Numerical simulation of soot formation in a turbulent flame with a Monte Carlo PDF approach and detailed chemistry*, Combust. Sci. Tech. 158(1) (2000), pp. 407–438.
[26] A. Wang and M.F. Modest, *Photon Monte Carlo simulation for radiative transfer in gaseous media represented by discrete particle fields*, J. Heat Transfer 128(10) (2006), pp. 1041–1049.
[27] A. Wang and M.F. Modest, *Spectral Monte Carlo models for nongray radiation analyses in inhomogeneous participating media*, Int. J. Heat Mass Transfer 50(19-20) (2007), pp. 3877–3889.

[28] A. Wang, M.F. Modest, D.C. Haworth and L. Wang, *Monte Carlo simulation of radiative heat transfer and turbulence interactions in methane/air jet flames*, J. Quant. Spectrosc. Radiat. Transfer 109(2) (2008), pp. 269–279.
[29] P.J. Coelho, *Numerical simulation of the interatction between turbulence and radiation in reactive flows*, Prog. Energy Combust. Sci. 33(4) (2007), pp. 311–383.
[30] R.S. Mehta, D.C. Haworth and M.F. Modest, *An assessment of gas-phase reaction mechanisms and soot models for laminar atmospheric-pressure ethylene–air flames*, Proc. Combust. Inst. 32(1) (2009), pp. 1327–1334.
[31] D. Veynante and L. Vervisch, *Turbulent combustion modeling*, Prog. Energy Combust. Sci. 28(3) (2002), pp. 193–266.
[32] D.C. Haworth, *Progress in probability density function methods for turbulent reacting flows*, Prog. Energy Combust. Sci. 36(2) (2009), pp. 168–259.
[33] S. Subramaniam and S.B. Pope, *A mixing model for turbulent reactive flows based on Euclidean minimum spanning trees*, Combust. Flame 115(4) (1998), pp. 487–514.
[34] M. Muradoglu, P. Jenny, S.B. Pope and D.A. Caughey, *A consistent hybrid finite volume/particle method for the PDF equations of turbulent reactive flows*, J. Comp. Phys. 154(2) (1999), pp. 342–371.
[35] P. Jenny, S.B. Pope, M. Muradoglu and D.A. Caughey, *A hybrid algorithm for the joint PDF equation of turbulent reactive flows*, J. Comp. Phys. 166(2) (2001), pp. 218–252.
[36] S.V. Subramaniam and D.C. Haworth, *A PDF method for turbulent mixing and combustion on three-dimensional unstructured deforming meshes*, Int. J. Engine Research 1(2) (2000), pp. 171–190.
[37] Y.Z. Zhang and D.C. Haworth, *A general mass consistency algorithm for hybrid particle/finite-volume PDF methods*, J. Comp. Phys. 194(1) (2004), pp. 156–193.
[38] C.K. Law, *Comprehensive description of chemistry in combustion modeling*, Combust. Sci. Tech. 177(5) (2005), pp. 845–870.
[39] R.J. Kee, G. Dixon-Lewis, J. Warnatz, M.E. Coltrin and J.A. Miller, *A computer code package for evaluation of gas-phase, multicomponent transport properties*, Technical Report SAND86-8246, Sandia National Laboratory, 1986.
[40] R.J. Kee, F.M. Rupley and J.A. Miller, *CHEMKIN-II: A Fortran chemical kinetics package for the analysis of gas-phase chemical kinetics*, Technical Report SAND89-8009B, Sandia National Laboratories, 1989.
[41] H. Bockhorn, *Soot Formation in Combustion*, Springer Verlag, New York, 1994.
[42] P. Lindstedt, *Simplified soot nucleation and surface growth steps for non-premixed flames*, in *Soot Formation in Combustion: Mechanisms and Models*, H. Bockhorn, ed., Springer-Verlag, New York, 1994.
[43] K.M. Leung, R.P. Lindstedt and W.P. Jones, A simplified reaction mechanism for soot formation in nonpremixed flames, Combust. Flame 87(3-4) (1991), pp. 289–305.
[44] R.P. Lindstedt and S.A. Louloudi, *Joint-scalar transported PDF modeling of soot formation and oxidation*, Proc. Combust. Inst. 30(1) (2005), pp. 775–783.
[45] I.M. Kennedy, *Models of soot formation and oxidation*, Prog. Energy Combust. Sci. 23(2) (1997), pp. 95–132.
[46] M. Frenklach and H. Wang, *Detailed modeling of soot particle nucleation and growth*, Proc. Combust. Inst. 23 (1991), pp. 1559–1566.
[47] M. Frenklach and H. Wang, *Detailed mechanism and modeling of soot particle formation*, in *Soot Formation in Combustion: Mechanisms and Models*, H. Bockhorn, ed. Springer-Verlag, New York, 1994.
[48] K.G. Neoh, J.B. Howard and A.F. Sarofim, in *Particulate Carbon: Formation During Combustion*, Siegla D.C. and G.W. Smith, eds., Plenum Press, New York, 1981, p. 261.
[49] M. Frenklach, *Method of moments with interpolative closure*, Chem. Eng. Sci. 57(12) (2002), pp. 2229–2239.
[50] J. Appel, H. Bockhorn and M Frenklach, *Kinetic moldeing of soot formation with detailed chemistry and physics: Laminar premixed flames of* C_2 *hydrocarbons*, Combust. Flame 121(1-2) (2000), pp. 122–136.
[51] H. Wang, D.X. Du, C.J. Sung and C.K. Law, *Experiments and numerical simulation on soot formation in opposed-jet ethylene diffusion flames*, Proc. Combust. Inst. 26 (1996), pp. 2359–2368.

[52] L. Wang, D.C. Haworth, S.R. Turns and M.F. Modest, *Interactions among soot, thermal radiation, and NOx emissions in oxygen-enriched turbulent nonpremixed flames: A CFD modeling study*, Combust. Flame 141(1-2), (2005), pp. 170–179.
[53] P.J. Coelho, O.J. Teerling and D. Roekaerts, *Spectral radiative effects and turbulence/radiation interaction in a non-luminous turbulent jet diffusion flame*, Combust. Flame 133(1-2) (2003), pp. 75–91.
[54] L. Tessé, F. Dupoirieux and J. Taine, *Monte Carlo modeling of radiative transfer in a turbulent sooty flame*, Int. J. Heat Mass Transfer 47 (2004), pp. 555–572.
[55] A.Y. Snegirev, *Statistical modeling of thermal radiation transfer in buoyant turbulent diffusion flames*, Combust. Flame 136(1-2) (2004), pp. 51–71.
[56] G. Li, *Investigation of turbulence–radiation interactions by a hybrid FV/PDF Monte Carlo method*, PhD thesis, The Pennsylvania State University, University Park, PA, 2002.
[57] H. Chang and T.T. Charalampopoulos, *Determination of the wavelength dependence of refractive indices of flame soot*, Proc. Roy. Soc. (London) A 430(1880) (1990), pp. 577–591.
[58] A. Kazakov and M. Frenklach, *Dynamic modeling of soot particle coagulation and aggregation: Implementation with the method of moments and application to high-pressure laminar premixed flames*, Combust. Flame 114(3–4) (1998), pp. 484–501.
[59] C.M. Sorensen, *Light scattering by fractal aggregates: A review*, Aerosol Sci. Tech. 35 (2001), pp. 648–687.
[60] A. Coppalle and D. Joyeux, *Temperature and soot volume fraction in turbulent diffusion flames: Measurements of mean and fluctuating values*, Combust. Flame 96(3) (1994), pp. 275–285.
[61] J.H. Kent and D. Honnery, *Soot and mixture fraction in turbulent diffusion flames*, Combust. Sci. Tech 54(1) (1987), pp. 383–398.
[62] M. Kalal and K.A. Nugent, *Abel inversion using fast Fourier transforms*, Appl. Opt. 27(10) (1988), pp. 1956–1959.
[63] L. Wang, N.E. Endrud, S.R. Turns, M.D. D'Agostini and A.G. Slavejkov, *A study of the influence of oxygen index on soot, radiation, and emission characteristics of turbulent jet flames*, Combust. Sci. Tech. 178(8) (2002), pp. 45–72.
[64] N.E. Endrud, Soot, *Radiation and pollutant emissions in oxygen-enhanced turbulent jet flames*, Master's thesis, The Pennsylvania State University, University Park, PA, 2000.
[65] R.V. Bandaru, *Experimental studies of the emission characteristics of nonpremixed gas–air flames of various configurations*, PhD thesis, The Pennsylvania State University, University Park, PA, 2000.
[66] A. Wang, *Investigation of turbulence–radiation interactions in turbulent flames using a hybrid finite volume/Monte Carlo approach*, PhD thesis, The Pennsylvania State University, 2007.